Magneto: Joint Angle Analysis Using an Electromagnet-Based Sensing Method

Amanda Watson
University of Pennsylvania
aawatson@seas.upenn.edu

Andrew Lyubovsky
William & Mary
amlyubovsky@email.wm.edu

Kenneth Koltermann
William & Mary
kkoltermann@cs.wm.edu

Gang Zhou
William & Mary
gzhou@cs.wm.edu

ABSTRACT

Joint angle analysis facilitates research into injury prevention, rehabilitation, and activity monitoring. Sensors used in such analysis must be unobtrusive, accurate, and if used for motion, capable of monitoring fast-paced, dynamic motions. To effectively contribute to these applications, we created a body-mounted electromagnet-based sensing system for joint angle analysis called Magneto. Our system is wireless, features a high sampling rate, is not subject to drift, and is unaffected by outside magnetic noise. Magnetic field readings are influenced by noise due to magnetic interference from the Earth's magnetic field, the environment, and nearby ferrous objects. Magneto uses the combination of an electromagnet and magnetometer to remove environmental interference from a magnetic field reading. We evaluated this sensing method to show its performance when removing the interference in three-movement dimensions, in six environments, and with six different cycling rates. Then, we localized the electromagnet with respect to the magnetic field reader in any direction within a 13.8 cm range with a relative error of 2.3% for the distance and an average error of 3.43° for the orientation angle. We applied Magneto in a pilot study: calculating elbow flexion angles. In this study, we calculated elbow flexion angles to the nearest 15° with 93.8% accuracy.

CCS CONCEPTS

• **Hardware → Sensor applications and deployments**.

KEYWORDS

Wearable Technology, Electromagnet, Magnetometer

1 INTRODUCTION

Joint angle analysis has been a significant research focus in the field of body motion tracking and modeling because knowledge of joint angles can be used for preventing injuries, decreasing rehabilitation time after injury, and accurate activity monitoring. Wearable sensors are commonly used for monitoring body motion and joint angles due to the advantages provided by direct bodily contact. These sensors are often used to monitor patient adherence to rehabilitation programs and assess patient recovery progress both inside and outside of a medical facility. Any proposed sensor for joint monitoring must be unobtrusive, accurate, and capable of accurately monitoring dynamic, fast-paced motions in order to be effective in healthcare applications.

Magnetic field sensors are affordable, low power sensors that are incorporated into many of the devices we use today including smartphones, smartwatches, and smart home devices. They allow large scale sensing of the Earth's magnetic field, magnetic anomalies, orientation, and distance. They can also be combined with magnets to allow smaller scale sensing, and have even been incorporated into wearable devices to track joint angles [67], body motions [31], and gestures [46]. A drawback of these sensors is that they fall victim to magnetic interference from the Earth's magnetic field, the environment, and nearby ferrous objects. Approaches used to protect a sensor from this magnetic interference include but are not limited to: using a hardware shield, using a magnet that is strong enough to eclipse all other fields or using multiple magnetic sensors. In this work, we address this drawback to improve upon joint angle tracking using this sensor.

In this paper, we address the following research questions:

RQ1: How can we eliminate environmental interference from a magnetic field reading?
RQ2: How can we localize an electromagnet given a purified magnetic field reading?
RQ3: How do we use electromagnet localization to determine joint angles?

To answer our first research question, we developed a method to remove environmental interference. First, we designed a small electromagnet that could produce a strong electromagnetic field. Then, we cycled the electromagnet between on and off states at a high frequency, allowing us to treat the recorded magnetic field strength in both states via a magnetometer as near-simultaneous. While the reading in both states has environmental interference, the on state reading has the environment with the magnetic field

from the electromagnet; the off state reading only has just the environment. Comparing the two removes environmental interference and provides a purified magnetic field reading of the electromagnet.

To answer our second research question, we localized the electromagnet given the purified magnetic field reading. For any purified reading, there is a set of location and orientation pairs representing the possible locations of the electromagnet. To calculate this set, we discuss the relationship between the magnetometer reading and the magnet's orientation and explain how to calculate a single location and orientation pair for the electromagnet. Then, we discuss the set of location and orientation pairs for a magnetic field reading.

To answer our third research question, we conducted a pilot study on elbow flexion angles and explored the possibilities of other applications in which Magneto can be used. First, we conducted a user study consisting of 13 participants in which we examined 12 different elbow flexion angles for a total data set of 650 measured angles. We processed the data and calculated the angles using a triangular representation and polynomial regression model. Then, we discussed further applications for which Magneto can be used.

Researchers have investigated using magnets to measure body motion [31, 45, 46, 60, 67]. While these works have successfully measured body motion, they did not account for the influence of environmental interference. This suggests that any change in the magnetic field reading would be interpreted as a change in body motion. With Magneto, we are able to remove the environmental interference and purify the electromagnetic signal so that any change in the magnetic field reading results from a change in the localization of the electromagnet. Additionally, magnetic field sensors have been used to sense motion in an environment [11, 50, 58]. These sensors use the magnetic field of the Earth as a reference point and are also susceptible to electromagnetic interference from nearby ferrous objects. Magneto is also able to remove electromagnetic interference produced by such objects.

Our contributions are summarized as follows:

(1) We developed a method that removes environmental interference from a magnetic field reading. We evaluated this method to show its performance when removing the interference in three movement dimensions, in six environments, and with six different cycling rates.

(2) We designed an algorithm that allows us to localize a magnet with respect to a magnetic field reader. Our algorithm calculated orientation of the magnet with an average error of 3.43° and distance from the reader to the magnet with an average error of 2.34% within a range of 13.8 cm from the magnetic field reader.

(3) We conducted a pilot study to evaluate Magneto on its ability to measure elbow flexion angles. We conducted a user study where we recorded 650 elbow flexion angles from 13 participants in which we examined 12 different elbow flexion angles for a total data set of 650 angles. Overall, our method saw an accuracy of 93.82% when classifying elbow flexion angles to the nearest 15° angle and an average error of 2.52°.

The remainder of this paper is structured as follows: First, we motivate our work by discussing our Related Work. Second, we introduce our Magneto Hardware Design by explaining the components and the construction of our electromagnet. Third, we describe the method that we used to eliminate environmental interference. Fourth, we explain the process that we use to localize the electromagnet with respect to our magnetic field reader. Fifth, we describe the application scenarios that Magneto can be used in and conduct two pilot studies. Finally, we discuss our Future Work and we wrap up with our Conclusion.

2 RELATED WORK

2.1 Human Motion Capture

Research in human motion capture is divided into two approaches: vision-based and non-vision-based. Early vision-based approaches [49, 71, 72, 75] used intensity images from RGB cameras, which were sensitive to lighting conditions. More recently, vision-based approaches make use of depth images from RGB-D cameras [19]. These cameras [59, 82] require markers worn on the body and/or specialized hardware placed in the recording environment. Markerless techniques [6, 8, 20] are non-intrusive and do not interfere with the subject or environment but require specific camera and human body positioning. None of the mentioned techniques used in vision-based approaches are portable and thus require a camera to be in a fixed location during motion human capture. These techniques are also affected by lighting conditions and obstructions making them non-optimal for use in ubiquitous scenarios. Magneto is unaffected by lighting conditions and obstructions making it valuable in situations where vision-based methods fail.

Non-vision-based approaches attach various sensors to the human body to determine the orientation of selected body parts. These sensors include but are not limited to: conductive textile sensors [44, 73, 81], flexible conductive polymers [7, 61], ultrasonic sensors [66], optical sensors [74, 77], liquid metal sensors [52, 54], potentiometers [22], acoustic sensors [79], flex sensors [5, 80], wireless signals [2, 65]. The most widely used wearable sensor is the inertial measurement unit (IMU) [12, 26, 33, 39, 76] as it is small, inexpensive, and widely tested making it the state-of-the-art for non-vision-based motion capture. While these qualities make these sensors appropriate for ubiquitous scenarios, IMU motion capture systems suffer from integration drift [25]. Common solutions to this issue include interpreting information from other sensors like GPS or WiFi signals to correct for this drift. Other solutions attempt to incorporate information related to the task being performed to reset the IMU's reading at specific points [48]. While solutions [34, 78] have been proposed to correct this drift, computation time and load have been increased, and often rely on less accurate sensor measurements or knowledge about specific application scenarios. In certain situations IMUs are known to Magneto avoids the problem of integration drift as our system does not accumulate a drift error. We compare our system to IMUs and stretch sensors on the elbow in Table 1. In this table, we compare the RMSE of Magneto with the RMSE of an IMU and a stretch sensor.

Sensor	Elbow Flexion/Extension
IMU [55] [13]	2.4°
Stretch Sensor [24] [41]	7.3°
Magneto	2.2°

Table 1: Sensor RMSE Comparison

2.2 Magnetics Based Sensing

Recently, magnets have been used in combination with magnetometers to monitor body motion by calculating the position and orientation of the object that the magnet resides on with respect to the magnetometer. Specifically, researchers have developed wearable devices using magnets and magnetometers to measure joint flexion and physical activity [31, 67]. Additionally, work has been done to attach magnets to the hand to monitor hand movements, postures and gestures [4, 15, 17, 28, 46, 51, 60]. Among all of these systems, the magnetic field reading is used to calculate distance and orientation. This requires the assumption that any change in magnetic field reading is a change in the distances and orientation between the magnetometer and the magnet. Because of this, outside magnetic fields can cause errors in the distance and orientation calculations. To solve this, the magnetometer can be calibrated for a specific environment, but to apply in ubiquitous scenarios, this calibration must be done every time the environment changes. Magneto accounts for the influence of outside magnetic fields by modulating the magnetic field of a wearable electromagnet.

Oscillation of electromagnetic fields has been used to dynamically remove the influence of outside magnetic fields from magnetic sensor readings in magnetic sensing scenarios [3, 9, 38, 63, 68]. Researchers have since applied this to surgical tracking [27, 40, 47, 84], virtual reality [35, 83], and HCI applications [18, 30, 51, 62]. Commercially, Polhemus [64], Engineering Systems Technologies [23], and NDI [56] have developed electromagnetic tracking systems in which a magnetic field is emitted by a source and magnetic sensors are attached to the tracked objects. Meskers et. al [53] used Flock of Birds developed by EST [23], a six-degree-of-freedom electromagnetic tracking device to measure shoulder positions. But the magnetic source requires a cable for power and is expected to remain in a fixed location limiting the environments in which they can be used to lab spaces or requiring additional setup at each new location. These systems also require multiple magnetic sensors to be placed on the body to calculate body positions or calculate a joint angle. They can fall victim to magnetic field distortion where the magnetic field will warp towards a nearby metal object [57]. Researchers have lessened this distortion through calibrations and additional algorithms [36, 85]. Magneto is a fully portable, wearable device consisting of a single magnetic sensor and a single electromagnet that is not limited to a static location and can thus be used for research outside of the lab. We designed our circuit for Magneto with two goals in mind. First, the device should be small so that it can be used in many different scenarios including as an on-body wearable. Second, the device should be capable of creating a strong and stable magnetic field so that it can be measured at a distance. To accomplish these two goals we created the circuit shown in Figure 1 with the following components:

3 MAGNETO HARDWARE DESIGN

Electromagnet: We built our own electromagnet as commercially available electromagnets were either too large to be comfortably worn on the body or their signal was too weak and their range did not suit our purposes. To build this electromagnet, we use the core of a 3.5 cm ferrite RF choke [69] and 28 gauge magnet wire[70]. Ferrite cores provide electromagnets with an increase in magnetic field
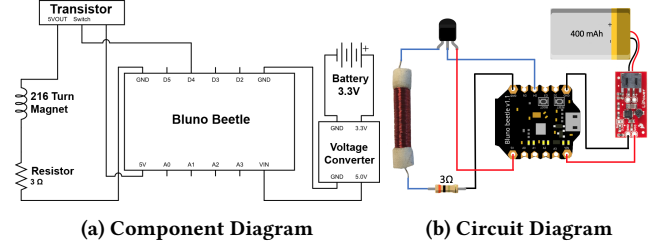

(a) Component Diagram

(b) Circuit Diagram

Figure 1: Magneto Hardware Diagrams

strength, and our magnet wire has a very thin insulation coating allowing us to wrap the wire around the RF choke more times in a smaller area. This makes our electromagnet stronger while preserving the small surface area. To build our electromagnet, we wound the magnet wire around the RF choke for many turns; a "turn" is defined as one full wrap of magnet wire around the core. Our resulting electromagnet shown in Figure 1b has three layers where the first, second, and third layers have 74, 72, and 70 turns, respectively. A

Figure 2: Cross Section

cross-section of the electromagnet is shown in Figure 2 to illustrate the layers of the electromagnet but is not drawn with accurate proportions. The resulting electromagnet has 216 total turns and a measured resistance of 1.3 ohms. In Section 4, we explain how we use these values to calculate the strength of our electromagnet.
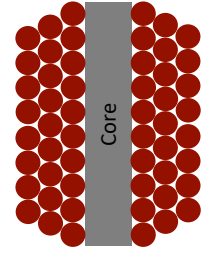
Microcontroller and Bluetooth Chip: To control our circuit, we chose the Bluno Beetle[10]. This device is currently the smallest bluetooth enabled Arduino on the market. This allows us to save space while providing all of the functionality that we need for our circuit. It outputs five volts which is important for the strength of the magnetic field of our electromagnet. This chip uses an ATmega328P processor and a CC2540 Bluetooth chip.
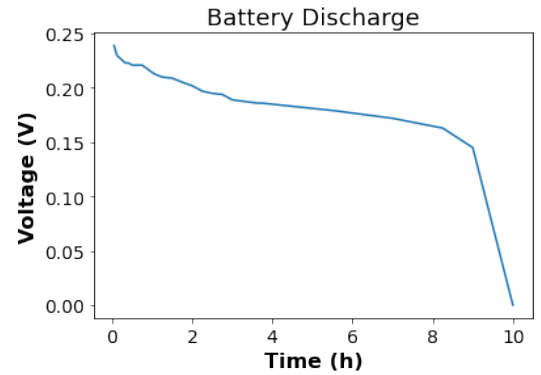

Figure 3: Battery Discharge

Power Supply: Our electromagnet requires at least a 5-volt power supply to create a magnetic field strong enough to be read by our magnetometer. The Bluno Beetle requires 5 to 8 volts to function properly. We used a 400mAh lithium-ion battery that only outputs 3.7 volts. To boost the 3.7 volts to 5 volts, we used a LiPower Boost Converter [43]. This battery provides our system with approximately 8 hours of battery life before the voltage begins to drop off, as shown in Figure 3.

Resistor: We tailored the resistance in our circuit to accomplish two goals: protect the Bluno microcontroller and prevent battery drain. We used a resistance of 3 ohms combined with our electromagnet at 1.3 ohms. This gives us a total of 4.3 ohms.

Transistor: We use an transistor as a switch in our circuit. Specifically, we used an NPN transistor that functions as a gate by either allowing current to pass or not pass. This facilitates our ability to turn the electromagnet on and off at a specified rate while still powering the electromagnet from the 5 volts. We could not use a digital pin from the Bluno as these output 3.3 volts.

These components are connected via wires and solder as shown in Figure 1. The device is then put into small and flexible fabric pouch so that the wires are protected and the electromagnet's signal is not restricted. This allows for an unobstructed magnetic field which provides for a high-quality reading as shown in the later sections of this paper.

Magnetic Field Reader: We use a magnetic field reader to record the magnetic field of our electromagnet. In this paper, we use a Shimmer 3 Sensor which houses a magnetometer that we use as our magnetic field reader. This sensor has a maximum sampling rate of 256 Hz and a sensing range of ±49 gauss.

4 ELIMINATION OF ENVIRONMENTAL INTERFERENCE

A problem with using a magnet and magnetometer combination as a sensor is the susceptibility to outside magnetic fields[16]. These magnetic fields include but are not limited to the magnetic field of the earth [29], ferrous metal objects [42], and other magnetized objects. These extraneous magnetic fields create a noisy signal that can make it hard to distinguish the movement of a magnet from the change in surrounding magnetic fields. To deal with this problem, we propose a method to eliminate the surrounding environment's magnetic field from the reading of the magnet. First, we explain our time cycle and cycling rate. Then, we discuss the method we use to remove the magnetic field of the environment.

Our signal is characterized by two states: ON and OFF. When the electromagnet is ON, we read the combination of the magnetic field of the electromagnet and the magnetic field of the surrounding environment. When the electromagnet is OFF, we only read the magnetic field of the surrounding environment. These states are shown in Figure 4. Next, we define a time cycle, t_{cycle}, that is the total time of a single ON state followed by a single OFF state, as shown in Figure 4. The total time spent in the ON state equal to the total time spent in the OFF state within each t_{cycle}. Then, we define the electromagnet's cycling rate to be the number of t_{cycle} per second.

Then for every ON and OFF state, there is a beginning and end. To find these points, we calculate an average line as shown in
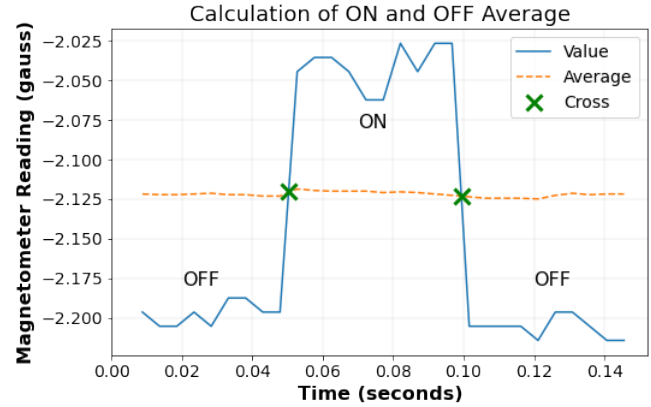

Figure 4: Average Calculation

Figure 4. This average consists of the data points in one time cycle. These data points are consecutive and evenly surround our targeted average value. Next, we mark each time the magnetometer reading crosses the average. The crosses are shown in Figure 4. Then, we label the point before the cross to be an end and the point after the cross to be a beginning. If the point is less than the value of the cross, we mark it as OFF. If the point is greater than the value of the cross, we mark it as ON. Once, we have the beginning and end to each ON and OFF state, we calculate the average to be our reading for that state. This is shown in Figure 5.
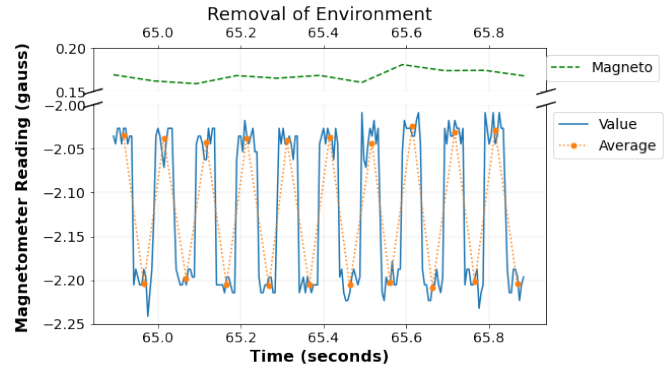

Figure 5: Averages and Environmental Noise Removal

Then we proceed to eliminate the environmental reading from our signal. To do this we take the average of the two OFF states that surround an ON state and subtract that from the ON state. We call this calculation M. It is shown in Figure 5. This is done for all three axes: x, y, and z. In some cases, the magnetic field shows up in only one or two of the axes. In these cases, we use the signal where the on and off switches are visible to set the ON and OFF starts and ends for the other axes.

4.1 Evaluation

We evaluate Magneto's ability to remove the environmental magnetic field readings by testing the following dimensions: orientation,

movement, magnetic field interference, and multiple environments. For these experiments, we set the electromagnet's cycling rate to 10Hz. We attached the electromagnet and the magnetometer to a board with eight centimeters between them as this is within the range of magnetic field of our electromagnet. This ensures that the distance and orientation of the electromagnet and magnetometer are constant with respect to each other, so any changes in readings must come from the manipulation of the board. So, any reading that the magnetometer picks up should be filtered out by our environmental elimination algorithm.
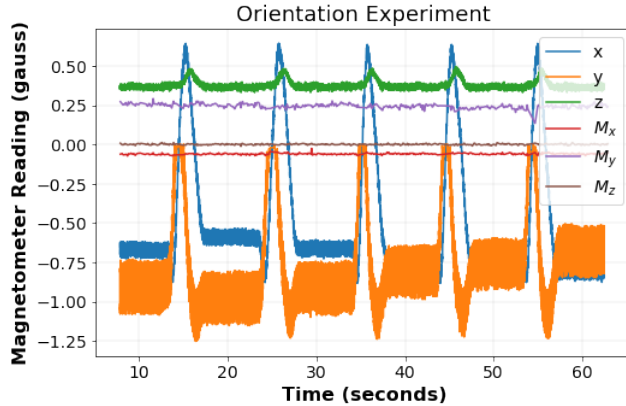

Figure 6: Orientation Experiment

Orientation Experiment: Each direction a magnetometer faces causes a different reading due to the magnetometer reading the earth's static but directional magnetic field. To test this dimension, we placed the board containing the electromagnet and magnetometer on an office chair. Then, we spun the office chair 360°. A single spin takes about five seconds to complete, and we stop the chair between spins. We repeated this experiment five times, and the results are shown in Figure 6. In this figure, x, y, and z are the raw sensor readings from the magnetometer, while M_x, M_y, and M_z have had the environment removed as described in the previous section. As seen in this figure, the magnetometer senses the spin of the chair. Since the electromagnet is not moving in respect to the magnetometer, we do not expect to see a variance in the readings of M_x, M_y, and M_z. These readings are all shown to be relatively flat in Figure 6. This confirms that we can effectively remove the spin read by the magnetometer. In this figure, we also see that the on and off of the electromagnet is not always seen in all three axes of the magnetometer. This is due to the fact that magnetic fields are vectors that are broken down into three components along the axes.

Movement Experiment: First, we tested how our sensor would react if it was facing different directions in a single environment. Next, it is important to move the sensor around in an environment. In this experiment, we vary the vertical and horizontal locations of the magnet in an environment. We also vary the speed at which we move through the environment. To test this dimension, we took our sensor attached to the board on a walk outside. The path we took is shown in Figure 7. We did this twice: once counterclockwise
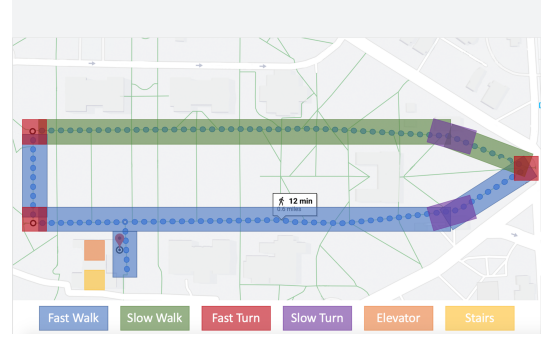

Figure 7: Walking Path

and once clockwise. Overall, it took approximately 25 minutes to complete both loops. On this walk, we completed several tasks: fast walk, slow walk, fast turn, slow turn, elevator, and stairs. We tested horizontal location and varying speeds with the fast walk, slow walk, fast turn, and slow turn. The fast walk averaged 5.6 miles per hour and the slow walk averaged 3.4 miles per hour. We define a fast turn to be a sharp turn lasting approximately two seconds while the slow turn was more gradual and occurred over nearly 20 seconds. We varied vertical locations and speeds by walking upstairs and riding in an elevator.
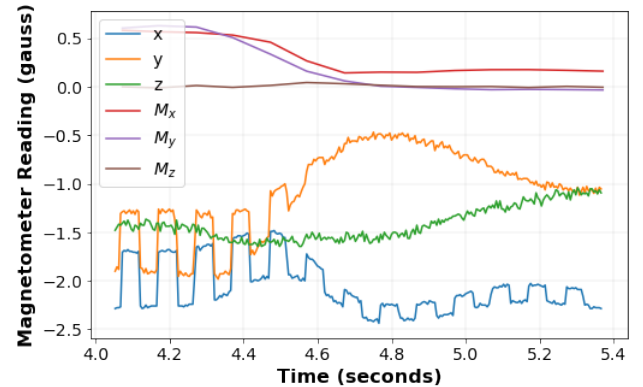

Figure 8: Fast Turn

Out of all of these tasks, we only observed a change in our Magneto reading during a fast turn. During these turns, we saw a slope in the reading of on and off state of the time cycle as shown in Figure 8. In the following sections, we see that increasing the cycling rate solves this problem. When more samples are collected, the slope through the on and off states diminishes so the reading can be more accurate. We also saw that the periodic motions associated with walking were removed since they did not cause a motion between our electromagnet and magnetometer. In all of the other tasks, we saw no change in our Magneto reading once the environment was removed.

Magnetic Interference Experiment: Magnetic interference is a common problem that affects magnetometers. This interference causes the readings of the magnetometer to be inconsistent and inaccurate.

Most interference is caused by iron present in the surrounding environment as it is a metal that can be magnetized. This interference can range from small static magnetic fields to distortions in the Earth's magnetic field. These distortions can warp the magnetic field in that area. This means that as a magnetometer moves through this field, we read changes with our magnetometer. Because of this, the distortion cannot be removed with a single calibration.
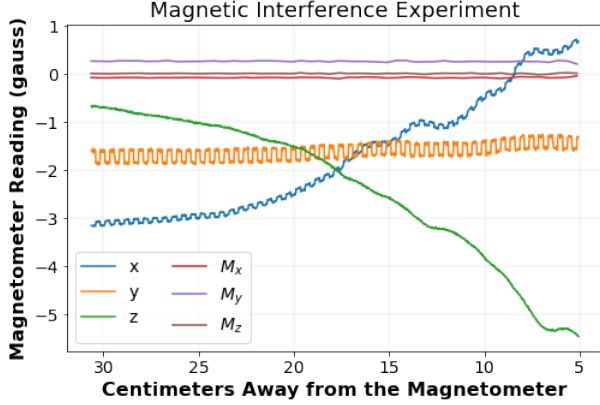

Figure 9: Magnetic Interference Experiment

To test the removal of these distortions, we introduce a strong outside magnetic field to our sensor: a stack of neodymium magnets. Neodymium magnets[37] are the strongest permanent magnets and are made from rare earth elements. We start these magnets 30 cm away from the magnetometer. We then move these magnets towards the magnetometer. The magnetometer reading is much larger than in the previous experiment due to the neodymium magnets. Inside of 5 cm, the magnetometer saturates, and it outputs error values. Even with the stronger magnetic field, we still see the on and off cycle of our electromagnet. This allows us to remove the reading of this magnet. We show this by the M_x, M_y, and M_z readings in Figure 9. These readings are comparable to what we see when there are not strong magnetic interferences. This shows that our device continues to function for its intended purpose even in the presence of strong and varied electromagnetic fields.

Multiple Environments: To ensure that our sensor could work in multiple types of environments, in the experiments above, we chose different locations. The orientation experiment was completed in our research lab. Our lab is next to the geology lab which produces a strong and static magnetic field. Our magnetometer reads the direction of the lab as North when it is in fact Southeast. There is also a higher reading in our lab than what is expected from the Earth's magnetic field. We completed our movement experiment outside, in the elevator, and in the stairwell and the Magnetic Interference experiment inside of a gymnasium. The gymnasium provides a large amount of environmental interference as many of the objects contained in a gym are made from ferrous materials. For example, many free weights are made from iron. These environments as well as their Gauss readings are shown in Figure 10. We noticed no difference in the final reading among all of the environments even though each environment had a different static magnetic field.
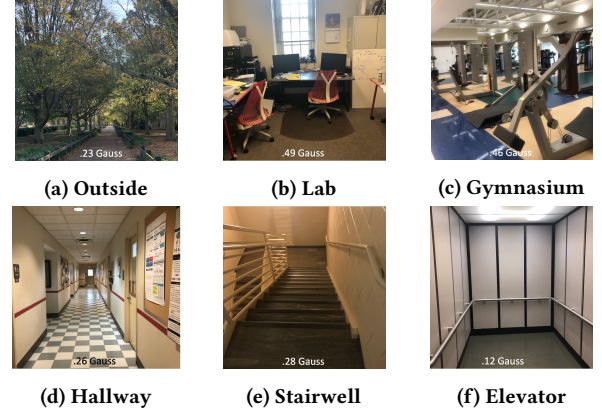

Figure 10: Environments Tested

Cycling Rate: In the experiments above, we used a cycling rate of 10 Hz. This is due to the fact that it is very clear to see the ON and OFF states with the human eye when we graphed our readings. To use our device in high-speed dynamic movements we must increase the cycling rate to get a clean reading on the movement. We tested the following cycling rates: 10 Hz, 20 Hz, 30 Hz, 40 Hz, 50 Hz, 100 Hz. We only tested up to 100 Hz as we are limited by our magnetometer sampling rate of 220 Hz. To understand if there is a degradation in the quality of our reading we did two studies. First, we compared the calculation of the means of the On and Off states using different cycling rates. Second, we looked at standard deviation in the raw signal in the On and Off states using different cycling rates.

Cycling Rate	Mean	Std Dev
10 Hz	0.0000	0.0121
20 Hz	0.0056	0.0157
30 HZ	0.0081	0.0183
40 HZ	0.0109	0.0211
50 HZ	0.0149	0.0372
100 HZ	0.0167	0.0533

Table 2: Cycling Rate Analysis

To compare the calculation of the means of the On and Off states using different cycling rates, we recorded 100 time cycles at 10 Hz. We then calculated the means of the ON and OFF periods using the number of expected data points in faster cycling rates. Then, we calculated the difference from the original mean. We show the average of the differences in the mean for all 100 time cycles in Table 2. As you can see, there is a small but steady degradation in the signal as the cycling rate increases. Next, we ensured that a faster cycling rate did not affect the edges of the On and Off states. To do this, we calculated the standard deviation in the raw signal in the On and Off states using different cycling rates. We recorded 100 cycles at each cycling rate. We show the results of this in Table, 2. We saw that the standard deviation steadily increased as the cycling rate increased. With further analysis into this data, we saw spikes at the beginning of the On and Off states. We discuss techniques to remove these spikes and to further increase the cycling rates in the Future Work Section.
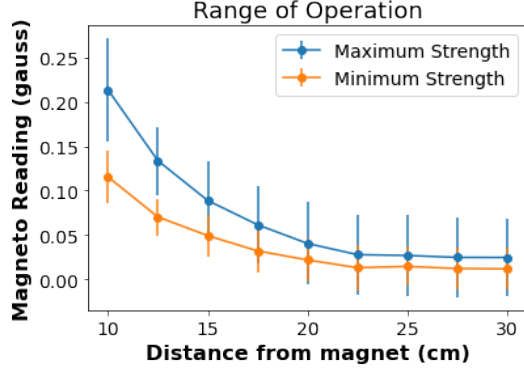
Figure 11: Magneto Sensing Range

*Magneto Sensing Range:*For many of the experiments above, we fixed the distance between the electromagnet and magnetometer to be eight centimeters. This was due to the fact that there was a strong, easy to recognize signal at this distance. We further explore the sensing range of our device by measuring the strength of the signal as it moves away from the magnetic field sensor. Given a more sensitive magnetic field sensor, a more accurate reading at further distances can be gathered. We show the results of our distance experiment in Figure 11. We start at ten centimeters away from the device because, in the previous experiments, we tested and validated eight centimeters away. Because a magnetic field is not uniform, the sensor reading depends on the orientation of the magnet. We show two orientations of the magnet in our figure. The first orientation maximizes the strength of the magnetic field and the second orientation minimizes it. This figure presents the entire range of magnetic field strengths for a given distance.

5 LOCALIZATION OF THE ELECTROMAGNET

For any reading recorded by the magnetometer, there is a set of location and orientation pairs for the electromagnet. To calculate these, we first discuss the relationship between the reading and the orientation. Then, we explain how to calculate a single location and orientation pair. Finally, we discuss the entirety of the set of location and orientation pairs for the electromagnet.

5.1 Magnetic Field

Magnets are described as dipoles, with one end of a magnet being a north pole and the other being a south pole. The opposite poles attract one another, and identical poles repel each other. Electromagnets are magnets with adjustable strength that can be turned on and off. A two-dimensional representation of the magnetic field surrounding our magnet is shown by the dotted blue lines in Figure 12. The three-dimensional representation would show this same magnetic field rotated around the magnet. This means that rotating the magnet would not change the magnetic field reading.

Magnetic fields around a magnet can be modeled given a magnet's strength with the assumption that a magnet is a perfect dipole. For any location around a magnet, we read a magnetic field (B) that reflects the distance (r) and angle (θ_N) from the north pole of the magnet. We show this in Figure 12. Since magnetic fields depend
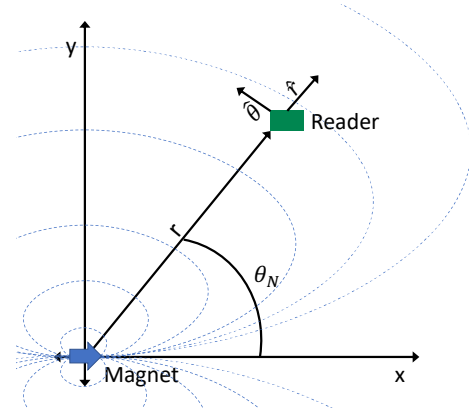

Figure 12: Magnetic Field from the Perspective of the Magnet

heavily on the angle θ_N, we use polar coordinates to describe the magnetic field reading. We represent the direction from the magnet to the reader as $\hat{r}$ and the direction perpendicular to that as $\hat{\theta}$ [21]. So, given a distance (r) and angle (θ_N), we can calculate the magnetic field (B) at the location (r, θ_N). $\frac{\mu_0 |m|}{4\pi}$ is a constant that depends on the materials and construction of the electromagnet. We can represent this with the following polar equation:

$$B(r, \theta_N) = \frac{\mu_0 |m|}{4\pi r^3} \left(2\cos\theta_N \, \hat{r} + \sin\theta_N \, \hat{\theta} \right) \qquad (1)$$

The description of the variables used in Equation 1 are shown in the following Table:

Variable	Definition
B	Magnetic field strength at the center of the core in Teslas
r	Distance from the reader to the magnet
θ_N	Angle of the north of the magnet
μ_0	Constant of magnetic permeability of free space: $4\pi * 10^{-7}$
$|m|$	Magnetic moment: current * area of loop * number of turns
$\hat{r}$	Direction from the magnet to the reader
$\hat{\theta}$	Direction perpendicular to $\hat{r}$

Table 3: Equation 1 Variable Definitions

For our purposes, we are given a magnetic field reading and want to calculate the distance (r) and orientation (θ_N) of the magnet. We explain these calculations with the aid of Figure 13. First, we put the reader at the origin of the coordinate system of the reader. The reader reads a vector, B. Given this reading, we can calculate θ_B which is the angle between vector B and the x axis. Then we assume the electromagnet is somewhere on a line that goes through the origin. This is represented by line L in Figure 13. θ_r is the angle between line L and vector B which can be calculated by finding the angle between two vectors. Since we know that θ_r is the angle between B and $\hat{r}$ in Figure 12, we can calculate the direction of the electromagnet's north with the following equation:
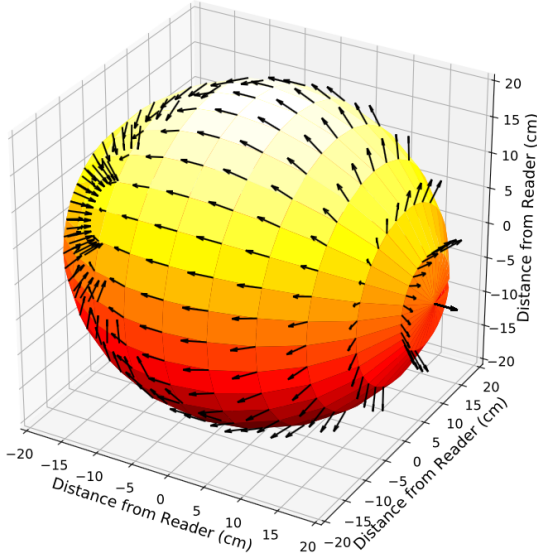
$$\theta_N = arctan(2tan\theta_r) \qquad (2)$$
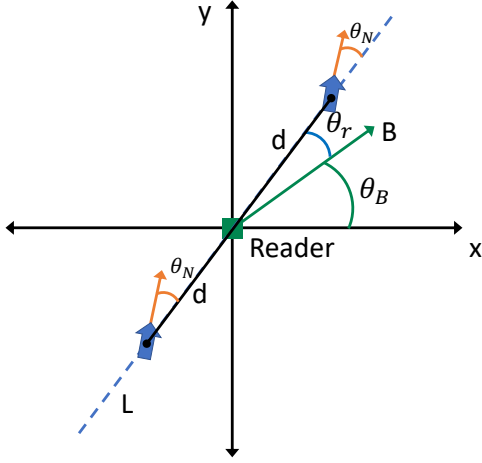
Figure 13: Magnet Position from the Perspective of the Reader

θ_N is the north for a magnet located anywhere on line l. Now that we know θ_N, we calculate the electromagnet's north with respect to the x axis. This is represented by θ_X, where

$$\theta_X = \theta_N + \theta_r + \theta_B \tag{3}$$

Then, we calculate the distance(r), via a derivation of Equation 1:

$$r = \sqrt[3]{\frac{\mu_0|m|}{4\pi|B|}\left(4cos^2\theta_N + sin^2\theta_N\right)^{\frac{1}{2}}} \tag{4}$$

Figure 14: Ellipsoid of Location and Orientation Pairs

This gives us the distance away from the origin on line L where the magnet is located. So, our magnet can be located in two locations

denoted by the points on line L as shown in Figure 13. Then we repeat this for every possible line through the origin. This gives us a set of location and orientation pairs around the reader in the shape of an ellipsoid as shown in Figure 14. In this example, we show the ellipsoid given by the magnetic field pointed in the positive x direction on the same coordinate system as the reader. We discuss how to use this in the Application Scenarios Section.
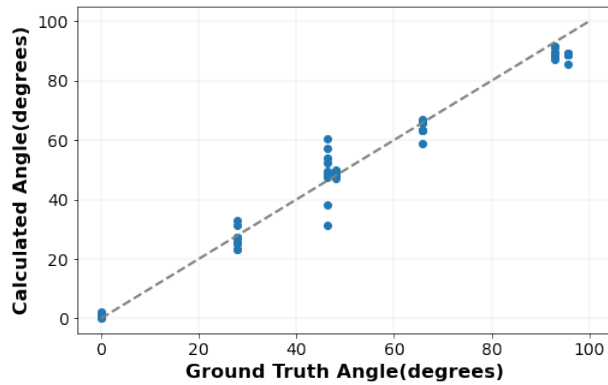
5.2 Evaluation

We calculated two variables to localize our electromagnet with respect to a magnetometer: distance and orientation. We evaluate the accuracy of the calculation of these variables. We set up our experiment with the magnet and the magnetometer in a grid, as shown in Figure 15. We left the electromagnet in a single location since the Shimmer Sensor is easier to move since it is housed in a case. This setup is in the same pattern as Figure 12 where the reader moves around the electromagnet. To perform this experiment, we created a grid in 5 cm by 5 cm blocks as shown in Figure 15. The distance measurements are offset in the x axis by a half centimeter as the magnetometer location in the Shimmer Sensor is not directly in the center of the device. We move the Shimmer Sensor to the center of each box for 30 seconds. We also record the ground truth values for our distance and orientation for that reading. These ground truth values are shown in each box in Figure 15. We do not test the other three quadrants around the magnet in this experiment as the distance calculations reflect over the x and y axis and the angles reflect over the x.

Figure 15: Experimental Setup

In this experiment, we process the data by removing the environment and then calculating the distance and orientation. As before, this gives us a set of data points in the shape of an ellipsoid. When we compare our calculated distance and orientation to our actual values, we assume we know the line L that the magnet is on. This comparison provides allows us to evaluate the accuracy of the set of distance and orientation pairs in the ellipsoid. Due to the limitations of our sensor, if we do not know how the electromagnet and reader move in relation to each other, then we do not know the actual location of the sensor. But for these instances, we do have a range of distances for which the electromagnet can be

(a) Orientation Results
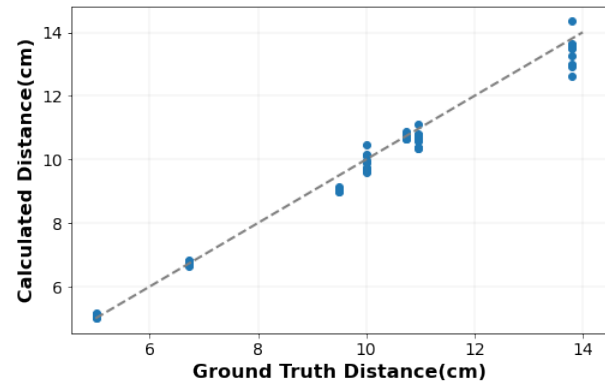
(b) Distance Results

Figure 16: Distance and Orientation Results

located. First, we evaluated the calculation of the orientation of the electromagnet. Overall, we have an average error per orientation calculation of 3.43° with a standard deviation of 3.28°. We further evaluate this with the use of Figure 16a. The orientations with the biggest difference in calculated value are the positions at which the magnetometer is the furthest away from the electromagnet. Second, we examined the distance between the electromagnet and the reader. We calculated the relative error of the distance to be 2.34% with a standard deviation of 2.03%. As we can see in Figure16b, the distance calculations are more accurate the closer the magnetometer is to the magnet. This means that the stronger our electromagnet, the more accurate our distance and orientation calculations will be at a distance. We discuss ways to increase the strength of our electromagnet in the Future Work Section.

6 APPLICATION SCENARIOS

Magneto can be used in many different application scenarios. It can also be used alongside other sensors to improve its performance. For example, IMUs are subject to drift which worsens the longer they are used. The IMU can be paired with Magneto to validate its readings to improve long-term performance by identifying when drift occurs. The magnetometer in the IMU can even be used by Magneto for data collection, thus only requiring an additional electromagnet. The key metrics that we compute are distance and orientation of the magnet, but to fully localize the magnet, we must know how the magnet and reader move in respect to one another. This setup lends itself to body motion application scenarios as we can set up our magnet and magnetometer equidistant from a joint. Then, because we know the biomechanics of the joint, we can calculate the exact localization of the magnet. This allows us to monitor, joint angles, speed of motion, and even gestures.

In situations where there is not a central joint, we can still localize the magnet if there is a restricted range of motion between the magnet and the reader. For example, over the lifetime of a spring, it stretches out until it is no longer useful. Magneto can be used to determine the length of the spring as its length would change over time. This would also hold true for strain sensors since in general, these sensors stretch out. Magneto could be used to sense the distance changed as the item wears out. Something of note is

that while our magnet or reader would need to be on the device, nothing would need to physically connect them. So there would be free space so the Magneto would not interfere with mechanisms of the device being measured.

Magneto can be used for position sensing and object tracking. Without knowledge of the relationship between the magnet and the magnetometer, a general position of the magnet can be derived, but it is limit the distance to a specific range from the magnetometer. If we know the relationship between the two devices, for example, if the magnet is always facing the magnetometer, the exact position can be derived with accuracy. This could be useful in situations such as tracking an object being manipulated in a person's hand.

To demonstrate how Magneto can be used in application scenarios, we conducted a pilot study: elbow flexion angle calculation. We describe our user study, process to calculate elbow flexion angles, and evaluate our calculation of the elbow flexion angles in a user study with thirteen participants.

6.1 Elbow Flexion Angle Pilot Study

We evaluated Magneto in an on-body scenario: elbow flexion angles. In this scenario, we calculated elbow flexion angles from the distance between the electromagnet and the magnetometer. First, we describe the equipment that we use. Second, we detail the parameters of our study and the demographics of our participants. Then, we explain the process used to calculate elbow flexion angles from a magnetometer reading. Finally, we evaluate our elbow angle calculation results.
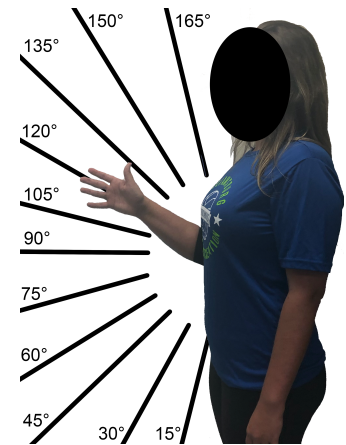

Figure 17: Elbow Study Setup

Equipment: To perform our IRB approved user study, we collected data on participants' elbow flexion angles. We collected magnetometer data that was influenced by our electromagnet's signal and ground truth angles. We used a Shimmer Sensor [14] magnetometer in conjunction with their data collection application to record data. This application was run on a Google Pixel 3 smartphone connected to the Shimmer Sensor via Bluetooth. We used a Medigauge digital goniometer [1], which is commonly used to measure joint angles and is accurate to the nearest 0.5°, to measure our ground truth angles. We marked the angles on a poster board to simplify the data recording process as shown in Figure 17. This means that our participants only needed to touch the line on the board for each angle instead of measuring each angle individually.
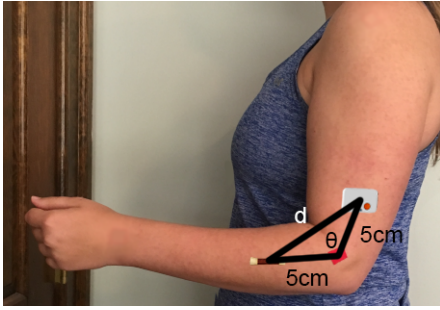

Figure 18: Elbow Angle Calculation

Parameters: When a participant arrived, we asked them to fill out a questionnaire. In this questionnaire, we asked for the following statistics: age, gender, height, weight, and any details of past elbow injuries or surgeries. Then we asked the participants to put on an elbow sleeve that contains our device and a Shimmer Sensor as shown in Figure 18. We positioned the sleeve so that the electromagnet is five centimeters below the elbow crease and the Shimmer Sensor is five centimeters above. The magnet is positioned lengthwise on the arm and the north is pointing towards the hand. Then, we positioned the participant in front of the poster board with marked angles as shown in Figure 17. We asked the participant to touch each of the marks with the outside of their hand for five seconds. They repeated this five times on that arm and then did the same on the other arm. The normal range of motion for an elbow is 0° at full extension and 130° at full flexion [32]. We measured angles at 15° increments within the normal range of motion.

Demographics: In this study, we had seven female and six male participants for a total of 13 participants. On average, the participants were 22.5 years of age with an age range of 18 to 33 years. All participants were in the range of normal for their body mass index (BMI). Everyone who participated in the study was free of elbow surgeries or recent injuries.

Elbow Angle Calculation: Next, we processed the data to calculate an elbow angle, θ. We started with raw magnetometer values and removed the environmental signal by using the method in Subsection 4 as shown in Figure 20. Then, we averaged the data for the five seconds that the participants held each elbow angle so that we had one reading per angle. Next, we calculated the ellipsoid of distance and orientation pairs between the electromagnet and
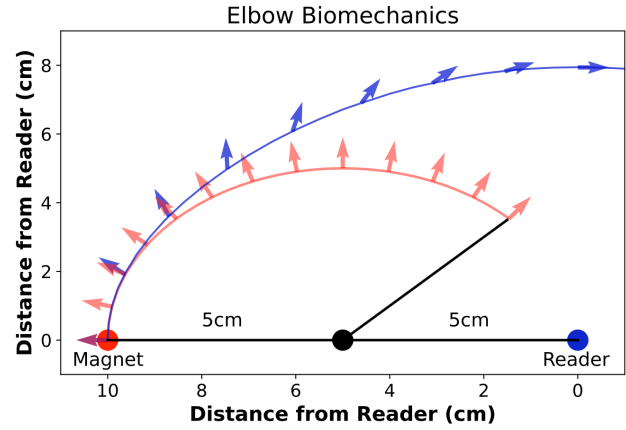

Figure 19: Elbow Biomechanics

the magnetometer by using the approach outlined in Section 5. To reduce the possible outcomes we leverage the biomechanics of the elbow. We limited the elbow to a single degree of motion. This means that the elbow moves within a single plane. So we show the single plane from the ellipsoid in Figure 19 as the blue arc with arrows. As the elbow bends, the electromagnet moves through the distance and orientation pairs shown by the red arc and arrows in Figure 19. In this Figure, the arrows represent the orientation of the north of the electromagnet and the arcs represent the strength of the magnetic field at that location. To calculate the exact orientation and direction of the magnet, we look to see where the red and blue arcs and arrows are identical. This gives us the location of the magnet. In our figure, this is shown by the purple arrow coming from the magnet.
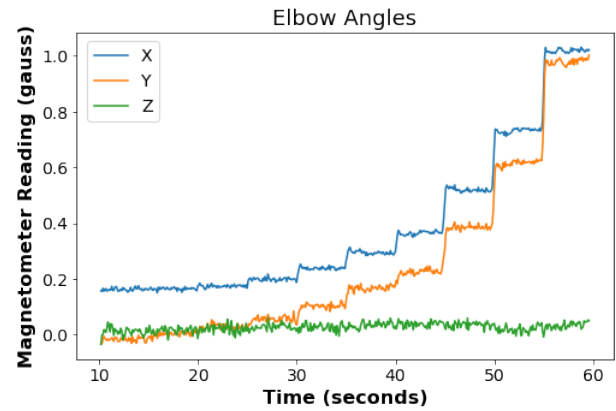
Figure 20: Environment-less Elbow Flexion Angles

Next, we calculated the distance from the magnet to the magnetometer in the method that we described in Section 5. From this distance, we calculated the elbow angle using the law of cosines on a triangle. We know the distance between the magnetometer and the elbow crease; and the electromagnet and the elbow crease as we set these to five centimeters on each side of the elbow crease.

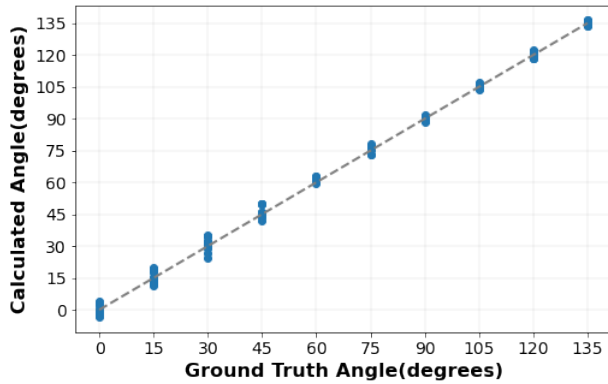Since we know all three sides of the triangle, we can calculate angle theta.

Figure 21: Angle Calculation Results

Results: We evaluated our elbow angle calculations on the 650 angles that we collected in our user study. Overall, we observed a 93.82% accuracy when classifying elbows to the nearest 15° and an average error of 2.52°. We show our results in Figure21. In this figure, we see that our angle calculations are much more accurate at the higher angles and that the first three angles have a much lower accuracy. To understand why, we look to Figure 20 and see that there is not much difference in the readings for angle 0°, 15°, and 30°. This is due to the fact that biomechanically there is more change in the distance in the larger angles. If we remove these three angles from our overall accuracy, we see a 97.07% accuracy and an average error of 1.95°.

7 DISCUSSION AND FUTURE WORK

Many things can be explored in future work. New algorithms can be examined for the elimination of the environment as well as for localizing the electromagnet. In this section, we focus on the ways that we can expand the sensing capabilities of our current electromagnet. First, we discuss applying Magneto to other joints. Next, we discuss how the strength of the electromagnet can be increased so that we can expand the working area of our device. Third, we discuss methods that can be used to increase the cycling rate. Lastly, we examined how we could use multiple electromagnets with a single magnetometer.

Magneto On the Shoulder: In the future, we plan to expand Magneto to additional joints on the body. We started this process by running preliminary tests on the shoulder. The shoulder is a much more complex joint when compared with the elbow, and the physiological complexion of the shoulder varies much more from person to person. Due to this complexity, the magnet and magnetometer must be placed further from one another, reducing the accuracy of the readings. In order to compensate for this, we increased the strength of the magnetic field. The shoulder angles were measured in three degrees of freedom: vertical motion of the arm, horizontal motion of the arm, and rotation of the arm (yaw, pitch, and roll respectively). With those constraints, we collected shoulder angles

on 16 users by placing the magnetometer on at the base of the trapezius and placing the magnet below the deltoid.

We modeled the predicted shoulder angle in each of the three degree of freedom using a neural network with three hidden layers. The shoulder angles had an average RMSE of 10° for yaw, 6° for pitch, and 5° for roll when modeling the shoulder angle on single users. When modeling on multiple users, and leaving one user out for testing, yaw had an average RMSE of 52°, pitch had an average RMSE 25°, and roll had an average RMSE of 30°. While testing on multiple users does not yet surpass the accuracy of IMU's, it shows promise for a future implementation of Magneto. In its current state, Magneto is user-specific on the shoulder due to errors caused by soft tissue differences from person to person. For example, let person A be 250 pounds, and person B 130 lbs and let the deltoid muscle be larger on person A. In this case, due to the way the magnet is placed, it will sit at a slightly different angle relative to the magnetometer leading to different readings from the same shoulder position, causing modeling errors.

In future work, the magnet placement should be fixed with respect to the magnetometer rather than being placed independently based on physiological structures. This will reduce the impact that differences in physiology have on Magneto's reading. In addition to the shoulder, other human joints can be modeled with Magneto. Furthermore, Magneto can be tested on nonhuman and even mechanical joints that have three degrees of freedom to show its promise as a sensor for joints with up to 3 degrees of freedom. This will address the complication caused by the variation in soft tissue from user to user.

Elbow Flexion Angle Analysis: In the elbow flexion angle experiment, we calculated the elbow angle based on the distance calculated from the magnetic field reading between the electromagnet and the magnetometer. We did not calculate the angle between the magnetometer and magnet directly from the magnetic field. We do believe it is possible and would allow for the calculation of elbow flexion angles without the need for the distance from the electromagnet to the joint and the magnetometer to the joint. We leave this up to future work to explore.

Increasing the Strength of the Electromagnet: We created our electromagnet in our lab using a choke and magnet wire. Our magnet has a working range of up to approximately 15 cm away from our magnetometer. While this worked for our applications, it would be helpful to have a stronger magnet with a larger range. Techniques to increase an electromagnet's strength are increasing the voltage or changing the materials the magnet is created with. Increasing the voltages comes with a trade-off, as Magneto would then have a higher energy consumption. This would require larger batteries and a different microcontroller potentially increasing the size of our wearable device. Changing the materials that the magnet is created with, on the other hand, will allow us to create a stronger magnetic field given the same current.

When the strength of the electromagnet is increased it becomes susceptible to oversaturation of the core. We experienced this when working with much higher voltage batteries, up to 24 volts. This causes a peak in the beginning of each ON and OFF state. This would need to be accounted for. A better core could also prevent oversaturation. A stronger magnet could saturate the magnetometer causing error values to be given. We observed oversaturation of

the electromagnet and the magnetometer. While these factors can be accounted for, we did not address them in this work and leave it for future work.

Increasing the Cycling Rate: To apply Magneto to fast-paced motions, such as those present in athletic movements, a faster cycling rate is required. In this work, we were limited by our magnetometer's sampling rate of 256 Hz. This restricted us to a cycling rate of up to 100Hz when working with our electromagnet. While we can run our sensor with a higher cycling rate, this will need to be tested with a different magnetometer to observe the quality of the signal. To increase the electromagnet's cycling rate, there are alternate methods to cycle the electromagnet. In this paper, we cycled the electromagnets through on and off. Another potential method that could be used is flipping the polarity of the electromagnet, i.e., switching the North and South poles of the magnet. Flipping the polarity of the electromagnet causes it to demagnetize at a faster rate than turning it off. This is a method has the potential to dramatically increase the cycling rate.

Multiple Electromagnets: Electromagnets of different strengths and frequencies can be investigated. This should provide the ability to record data from multiple electromagnets using only one magnetometer. This will allow for the sensing of multiple joints at once. For example, we could sense the motion of the shoulder and the elbow simultaneously with a strong enough electromagnet. Multiple electromagnets could even be used to sense parts of the body with many small joints such as the hands and fingers.

8 CONCLUSION

In this work, we presented Magneto, a sensing system for joint angle analysis. Magneto uses the combination of an electromagnet and magnetometer to remove environmental interference from magnetic field readings in a dynamically changing environment. Given this purified reading, we localized the electromagnet with respect to the magnetic field reader which allowed us to apply Magneto in a pilot study: elbow angle calculation where we calculated elbow angles to the nearest 15° with 93.8% accuracy.

ACKNOWLEDGMENTS

REFERENCES

[1] [n.d.]. Medigauge: Digital Protractor Goniometer for Medical applications. http://www.medigauge.com/digital-protractor-goniometer-for-medical-applications/
[2] Boyd Anderson, Mingqian Shi, Vincent YF Tan, and Ye Wang. 2019. Mobile Gait Analysis Using Foot-Mounted UWB Sensors. *Proceedings of the ACM on Interactive, Mobile, Wearable and Ubiquitous Technologies* 3, 3 (2019), 73.
[3] Peter Traneus Anderson. 2010. Ultra-low frequency electromagnetic tracking system. US Patent 7,761,100.
[4] Daniel Ashbrook, Patrick Baudisch, and Sean White. 2011. Nenya: subtle and eyes-free mobile input with a magnetically-tracked finger ring. In *Proceedings of the SIGCHI Conference on Human Factors in Computing Systems*. 2043–2046.
[5] Saba Bakhshi and Mohammad H Mahoor. 2011. Development of a wearable sensor system for measuring body joint flexion. In *2011 International Conference on Body Sensor Networks*. IEEE, 35–40.
[6] Kai Berger, Kai Ruhl, Yannic Schroeder, Christian Bruemmer, Alexander Scholz, and Marcus A Magnor. 2011. Markerless motion capture using multiple color-depth sensors.. In *VMV*. 317–324.

[7] Jeroen HM Bergmann, Salzitsa Anastasova-Ivanova, Irina Spulber, Vivek Gulati, Pantelis Georgiou, and Alison McGregor. 2013. An attachable clothing sensor system for measuring knee joint angles. *IEEE Sensors Journal* 13, 10 (2013), 4090–4097.
[8] Alessandro Bissacco, Ming-Hsuan Yang, and Stefano Soatto. 2007. Fast human pose estimation using appearance and motion via multi-dimensional boosting regression. In *2007 IEEE conference on computer vision and pattern recognition*. IEEE, 1–8.
[9] Ernest B Blood. 1990. Device for quantitatively measuring the relative position and orientation of two bodies in the presence of metals utilizing direct current magnetic fields. US Patent 4,945,305.
[10] Bluno [n.d.]. Bluno Beetle SKU:DFR0339. https://www.dfrobot.com/wiki/index.php/Bluno_Beetle_SKU:DFR0339
[11] Stephane Bonnet and Rodolphe Heliot. 2007. A magnetometer-based approach for studying human movements. *IEEE Transactions on Biomedical Engineering* 54, 7 (2007), 1353–1355.
[12] Vincent Bonnet, Claudia Mazza, Philippe Fraisse, and Aurelio Cappozzo. 2013. Real-time estimate of body kinematics during a planar squat task using a single inertial measurement unit. *IEEE Transactions on Biomedical Engineering* 60, 7 (2013), 1920–1926.
[13] Brice Bouvier, Sonia Duprey, Laurent Claudon, Raphaël Dumas, and Adriana Savescu. 2015. Upper limb kinematics using inertial and magnetic sensors: Comparison of sensor-to-segment calibrations. *Sensors* 15, 8 (2015), 18813–18833.
[14] Adrian Burns, Barry R Greene, Michael J McGrath, Terrance J O'Shea, Benjamin Kuris, Steven M Ayer, Florin Stroiescu, and Victor Cionca. 2010. SHIMMER–A wireless sensor platform for noninvasive biomedical research. *IEEE Sensors Journal* 10, 9 (2010), 1527–1534.
[15] Liwei Chan, Rong-Hao Liang, Ming-Chang Tsai, Kai-Yin Cheng, Chao-Huai Su, Mike Y Chen, Wen-Huang Cheng, and Bing-Yu Chen. 2013. FingerPad: private and subtle interaction using fingertips. In *Proceedings of the 26th annual ACM symposium on User interface software and technology*. 255–260.
[16] Howard Chen. 2017. The effects of movement speeds and magnetic disturbance on inertial measurement unit accuracy: the implications of sensor fusion algorithms in occupational ergonomics applications. (2017).
[17] Ke-Yu Chen, Kent Lyons, Sean White, and Shwetak Patel. 2013. uTrack: 3D input using two magnetic sensors. In *Proceedings of the 26th annual ACM symposium on User interface software and technology*. ACM, 237–244.
[18] Ke-Yu Chen, Shwetak N Patel, and Sean Keller. 2016. Finexus: Tracking precise motions of multiple fingertips using magnetic sensing. In *Proceedings of the 2016 CHI Conference on Human Factors in Computing Systems*. 1504–1514.
[19] Lulu Chen, Hong Wei, and James Ferryman. 2013. A survey of human motion analysis using depth imagery. *Pattern Recognition Letters* 34, 15 (2013), 1995–2006.
[20] Stefano Corazza, Lars Mündermann, Emiliano Gambaretto, Giancarlo Ferrigno, and Thomas P Andriacchi. 2010. Markerless motion capture through visual hull, articulated icp and subject specific model generation. *International journal of computer vision* 87, 1-2 (2010), 156.
[21] J.J. D. 1975. *Classical Electrodynamics*. John Wiley. https://books.google.com/books?id=fS62uQAACAAJ
[22] Luca Della Toffola, Shyamal Patel, Muzaffer Y Ozsecen, Ravi Ramachandran, and Paolo Bonato. 2012. A wearable system for long-term monitoring of knee kinematics. In *Proceedings of 2012 IEEE-EMBS International Conference on Biomedical and Health Informatics*. IEEE, 188–191.
[23] Engineering Systems Technologies 2020. Engineering Systems Technologies: trackSTAR/driveBay. https://est-kl.com/manufacturer/ascension/trakstar-drivebay.html
[24] Yu Enokibori and Kenji Mase. 2014. Human joint angle estimation with an e-textile sensor. In *Proceedings of the 2014 ACM International Symposium on Wearable Computers*. ACM, 129–130.
[25] Alessandro Filippeschi, Norbert Schmitz, Markus Miezal, Gabriele Bleser, Emanuele Ruffaldi, and Didier Stricker. 2017. Survey of motion tracking methods based on inertial sensors: A focus on upper limb human motion. *Sensors* 17, 6 (2017), 1257.
[26] Giancarlo Fortino and Raffaele Gravina. 2014. A cloud-assisted wearable system for physical rehabilitation. In *ICTs for Improving Patients Rehabilitation Research Techniques*. Springer, 168–182.
[27] Marvin P Fried, Jonathan Kleefield, Harsha Gopal, Edward Reardon, Bryan T Ho, and Frederick A Kuhn. 1997. Image-guided endoscopic surgery: results of accuracy and performance in a multicenter clinical study using an electromagnetic tracking system. *The Laryngoscope* 107, 5 (1997), 594–601.
[28] Chris Harrison and Scott E Hudson. 2009. Abracadabra: wireless, high-precision, and unpowered finger input for very small mobile devices. In *Proceedings of the 22nd annual ACM symposium on User interface software and technology*. 121–124.
[29] Kumar Hemant, Erwan Thébault, Mioara Mandea, Dhananjay Ravat, and Stefan Maus. 2007. Magnetic anomaly map of the world: merging satellite, airborne, marine and ground-based magnetic data sets. *Earth and Planetary Science Letters* 260, 1-2 (2007), 56–71.
[30] Jiawei Huang, Tsuyoshi Mori, Kazuki Takashima, Shuichiro Hashi, and Yoshifumi Kitamura. 2015. IM6D: magnetic tracking system with 6-DOF passive markers

for dexterous 3D interaction and motion. *ACM Transactions on Graphics (TOG)* 34, 6 (2015), 1–10.

[31] Todd J Hullfish, Feini Qu, Brendan D Stoeckl, Peter M Gebhard, Robert L Mauck, and Josh R Baxter. 2019. Measuring clinically relevant knee motion with a self-calibrated wearable sensor. *Journal of biomechanics* 89 (2019), 105–109.

[32] Felix H. Savoie III. [n.d.]. Elbow Anatomy & Biomechanics. https://www.orthobullets.com/shoulder-and-elbow/3078/elbow-anatomy-and-biomechanics

[33] Carolin Jakob, Patrick Kugler, Felix Hebenstreit, Samuel J Reinfelder, Ulf Jensen, Dominik Schuldhaus, Matthias Lochmann, and Bjoern Eskofier. 2013. Estimation of the Knee Flexion-Extension Angle During Dynamic Sport Motions Using Body-worn Inertial Sensors.. In *BodyNets*. Citeseer, 289–295.

[34] Antonio Ramón Jiménez, Fernando Seco, José Carlos Prieto, and Jorge Guevara. 2010. Indoor pedestrian navigation using an INS/EKF framework for yaw drift reduction and a foot-mounted IMU. In *2010 7th Workshop on Positioning, Navigation and Communication*. IEEE, 135–143.

[35] Wooyoung Kim, Jihoon Song, and Frank C Park. 2017. Closed-form position and orientation estimation for a three-axis electromagnetic tracking system. *IEEE Transactions on Industrial Electronics* 65, 5 (2017), 4331–4337.

[36] Volodymyr V Kindratenko and William F Sherman. 2005. Neural network-based calibration of electromagnetic tracking systems. *Virtual Reality* 9, 1 (2005), 70–78.

[37] K&J [n.d.]. K&J Magnetics - Neodymium Magnet Information. https://www.kjmagnetics.com/neomaginfo.asp

[38] Jack B Kuipers. 1980. SPASYN-an electromagnetic relative position and orientation tracking system. *IEEE Transactions on Instrumentation and Measurement* 29, 4 (1980), 462–466.

[39] Liu Kun, Yoshio Inoue, Kyoko Shibata, and Cao Enguo. 2011. Ambulatory estimation of knee-joint kinematics in anatomical coordinate system using accelerometers and magnetometers. *IEEE Transactions on Biomedical Engineering* 58, 2 (2011), 435–442.

[40] Katja M Langen, Twyla R Willoughby, Sanford L Meeks, Anand Santhanam, Alexis Cunningham, Lisa Levine, and Patrick A Kupelian. 2008. Observations on real-time prostate gland motion using electromagnetic tracking. *International Journal of Radiation Oncology* Biology* Physics* 71, 4 (2008), 1084–1090.

[41] Hyosang Lee, Jiseung Cho, and Jung Kim. 2016. Printable skin adhesive stretch sensor for measuring multi-axis human joint angles. In *2016 IEEE International Conference on Robotics and Automation (ICRA)*. IEEE, 4975–4980.

[42] James Lenz and S Edelstein. 2006. Magnetic sensors and their applications. *IEEE Sensors journal* 6, 3 (2006), 631–649.

[43] LiPower [n.d.]. LiPower - Boost Converter. https://www.sparkfun.com/products/10255

[44] Ruibo Liu, Qijia Shao, Siqi Wang, Christina Ru, Devin Balkcom, and Xia Zhou. 2019. Reconstructing human joint motion with computational fabrics. *Proceedings of the ACM on Interactive, Mobile, Wearable and Ubiquitous Technologies* 3, 1 (2019), 1–26.

[45] Y. Ma, Z. Mao, W. Jia, C. Li, J. Yang, and M. Sun. 2011. Magnetic Hand Tracking for Human-Computer Interface. *IEEE Transactions on Magnetics* 47, 5 (May 2011), 970–973. https://doi.org/10.1109/TMAG.2010.2076401

[46] Yinghong Ma, Zhi-Hong Mao, Wenyan Jia, Chengliu Li, Jiawei Yang, and Mingui Sun. 2011. Magnetic hand tracking for human-computer interface. *IEEE Transactions on Magnetics* 47, 5 (2011), 970–973.

[47] Robert A MacLachlan, RL Hollis, Joseph N Martel, LA Lobes Jr, and Cameron N Riviere. 2017. Toward improved electromagnetic tracking for handheld robotics. In *Proceedings of the 3rd International Conference on Mechatronics and Robotics Engineering*. 75–80.

[48] Maria Markovska and Ruben Svensson. 2019. Evaluation of drift correction strategies for an inertial based dairy cow positioning system.: A study on tracking the position of dairy cows using a foot mounted IMU with drift correction from ZUPT or sparse RFID locations.

[49] Marcin Marszalek, Ivan Laptev, and Cordelia Schmid. 2009. Actions in context. In *2009 IEEE Conference on Computer Vision and Pattern Recognition*. IEEE, 2929–2936.

[50] John E McFee, Robert O Ellingson, and Yogadhish Das. 1994. A total-field magnetometer system for location and identification of compact ferrous objects. *IEEE transactions on instrumentation and measurement* 43, 4 (1994), 613–619.

[51] Jess McIntosh, Paul Strohmeier, Jarrod Knibbe, Sebastian Boring, and Kasper Hornbæk. 2019. Magnetips: Combining fingertip tracking and haptic feedback for around-device interaction. In *Proceedings of the 2019 CHI Conference on Human Factors in Computing Systems*. 1–12.

[52] Yiğit Mengüç, Yong-Lae Park, Hao Pei, Daniel Vogt, Patrick M Aubin, Ethan Winchell, Lowell Fluke, Leia Stirling, Robert J Wood, and Conor J Walsh. 2014. Wearable soft sensing suit for human gait measurement. *The International Journal of Robotics Research* 33, 14 (2014), 1748–1764.

[53] CGM Meskers, HM Vermeulen, JH De Groot, FCT Van der Helm, and PM Rozing. 1998. 3D shoulder position measurements using a six-degree-of-freedom electromagnetic tracking device. *Clinical biomechanics* 13, 4-5 (1998), 280–292.

[54] Hadrien O Michaud, Joan Teixidor, and Stéphanie P Lacour. 2015. Soft flexion sensors integrating strechable metal conductors on a silicone substrate for smart

[55] Philipp Müller, Marc-André Bégin, Thomas Schauer, and Thomas Seel. 2016. Alignment-free, self-calibrating elbow angles measurement using inertial sensors. *IEEE journal of biomedical and health informatics* 21, 2 (2016), 312–319.

[56] NDI 2020. NDI: MedicalAurora. https://www.ndigital.com/medical/products/aurora/

[57] Mark A Nixon, Bruce C McCallum, W Richard Fright, and N Brent Price. 1998. The effects of metals and interfering fields on electromagnetic trackers. *Presence* 7, 2 (1998), 204–218.

[58] Karol J O'Donovan, Roman Kamnik, Derek T O'Keeffe, and Gerard M Lyons. 2007. An inertial and magnetic sensor based technique for joint angle measurement. *Journal of biomechanics* 40, 12 (2007), 2604–2611.

[59] F Ofli, Y Demir, E Erzin, Y Yemez, and AM Tekalp. 2007. Joint Correlation Analysis of Audio-Visual Dance Figures. In *2007 IEEE 15th Signal Processing and Communications Applications*. IEEE, 1–4.

[60] Steven Osman. 2017. Magnetic tracking of glove fingertips with peripheral devices. US Patent 9,665,174.

[61] E. Papi, I. Spulber, M. Kotti, P. Georgiou, and A. H. McGregor. 2015. Smart Sensing System for Combined Activity Classification and Estimation of Knee Range of Motion. *IEEE Sensors Journal* 15, 10 (Oct 2015), 5535–5544. https://doi.org/10.1109/JSEN.2015.2444441

[62] Farshid Salemi Parizi, Eric Whitmire, and Shwetak Patel. 2019. AuraRing: Precise Electromagnetic Finger Tracking. *Proceedings of the ACM on Interactive, Mobile, Wearable and Ubiquitous Technologies* 3, 4 (2019), 1–28.

[63] Valter Pasku, Alessio De Angelis, Guido De Angelis, Darmindra D Arumugam, Marco Dionigi, Paolo Carbone, Antonio Moschitta, and David S Ricketts. 2017. Magnetic field-based positioning systems. *IEEE Communications Surveys & Tutorials* 19, 3 (2017), 2003–2017.

[64] Polhemus 2020. Polhemus:Electromagnet Tracking 6DOF: Reliable Data, Repeatable Results. https://polhemus.com/applications/electromagnetics/

[65] Yongbin Qi, Cheong Boon Soh, Erry Gunawan, Kay-Soon Low, and Arash Maskooki. 2013. A novel approach to joint flexion/extension angles measurement based on wearable UWB radios. *IEEE journal of biomedical and health informatics* 18, 1 (2013), 300–308.

[66] Yongbin Qi, Cheong Boon Soh, Erry Gunawan, Kay-Soon Low, and Arash Maskooki. 2014. A novel approach to joint flexion/extension angles measurement based on wearable UWB radios. *IEEE journal of biomedical and health informatics* 18, 1 (2014), 300–308.

[67] Feini Qu, Brendan D Stoeckl, Peter M Gebhard, Todd J Hullfish, Josh R Baxter, and Robert L Mauck. 2018. A Wearable Magnet-Based System to Assess Activity and Joint Flexion in Humans and Large Animals. *Annals of biomedical engineering* 46, 12 (2018), 2069–2078.

[68] Frederick H Raab, Ernest B Blood, Terry O Steiner, and Herbert R Jones. 1979. Magnetic position and orientation tracking system. *IEEE Transactions on Aerospace and Electronic systems* 5 (1979), 709–718.

[69] Radioshack [n.d.]. 100μ H RF Choke: Radioshack. https://www.radioshack.com/products/radioshack-100-h-rf-choke. [Online; accessed 10-October-2019].

[70] Remington [n.d.]. Remington Industries 28SNSP.25 28 AWG Magnet Wire, Enameled Copper Wire, 4 oz, 0.0135" Diameter, 507' Length, Red. https://www.amazon.com/Remington-Industries-28SNSP-25-Enameled-Diameter/dp/B00I53B2TC/ref=sr_1_3?keywords=magnet+wire&qid=1563292790&s=gateway&sr=8-3. [Online; accessed 10-October-2019].

[71] Mikel D Rodriguez, Javed Ahmed, and Mubarak Shah. 2008. Action mach a spatiotemporal maximum average correlation height filter for action recognition. In *2008 IEEE conference on computer vision and pattern recognition*. IEEE, 1–8.

[72] Christian Schuldt, Ivan Laptev, and Barbara Caputo. 2004. Recognizing human actions: a local SVM approach. In *Proceedings of the 17th International Conference on Pattern Recognition, 2004. ICPR 2004.*, Vol. 3. IEEE, 32–36.

[73] Tien-Wei Shyr, Jing-Wen Shie, Chang-Han Jiang, and Jung-Jen Li. 2014. A textile-based wearable sensing device designed for monitoring the flexion angle of elbow and knee movements. *Sensors* 14, 3 (2014), 4050–4059.

[74] Ana S Silva, André Catarino, Miguel V Correia, and Orlando Frazão. 2013. Design and characterization of a wearable macrobending fiber optic sensor for human joint angle determination. *Optical Engineering* 52, 12 (2013), 126106.

[75] Suresh Singh and Cauligi S Raghavendra. 1998. PAMAS—power aware multiaccess protocol with signalling for ad hoc networks. *ACM SIGCOMM Computer Communication Review* 28, 3 (1998), 5–26.

[76] Odongo Steven Eyobu and Dong Seog Han. 2018. Feature representation and data augmentation for human activity classification based on wearable IMU sensor data using a deep LSTM neural network. *Sensors* 18, 9 (2018), 2892.

[77] Dragan Z Stupar, Jovan S Bajic, Lazo M Manojlovic, Miloš P Slankamenac, Ana V Joza, and Miloš B Zivanov. 2012. Wearable low-cost system for human joint movements monitoring based on fiber-optic curvature sensor. *IEEE Sensors Journal* 12, 12 (2012), 3424–3431.

[78] Makoto Tanigawa, Henk Luinge, Linda Schipper, and Per Slycke. 2008. Drift-free dynamic height sensor using MEMS IMU aided by MEMS pressure sensor. In *2008 5th Workshop on Positioning, Navigation and Communication*. IEEE, 191–196.

[79] Caitlin N Teague, Sinan Hersek, Hakan Töreyin, Mindy L Millard-Stafford, Michael L Jones, Géza F Kogler, Michael N Sawka, and Omer T Inan. 2016. Novel methods for sensing acoustical emissions from the knee for wearable joint health assessment. *IEEE Transactions on Biomedical Engineering* 63, 8 (2016), 1581–1590.

[80] Po T Wang, Christine E King, An H Do, and Zoran Nenadic. 2011. A durable, low-cost electrogoniometer for dynamic measurement of joint trajectories. *Medical engineering & physics* 33, 5 (2011), 546–552.

[81] Amanda Watson, Minglong Sun, Samhita Pendyal, and Gang Zhou. 2020. TracKnee: Knee angle measurement using stretchable conductive fabric sensors. *Smart Health* 15 (2020), 100092.

[82] Matthias Weber. 2008. A hybrid approach towards fully automatic 3D marker tracking. In *Proceedings of the 2008 ACM symposium on Virtual reality software and technology.* 243–244.

[83] Eric Whitmire, Farshid Salemi Parizi, and Shwetak Patel. 2019. Aura: Inside-out electromagnetic controller tracking. In *Proceedings of the 17th Annual International Conference on Mobile Systems, Applications, and Services.* 300–312.

[84] Guofang Xiao, Ester Bonmati, Stephen Thompson, Joe Evans, John Hipwell, Daniil Nikitichev, Kurinchi Gurusamy, Sébastien Ourselin, David J Hawkes, Brian Davidson, et al. 2018. Electromagnetic tracking in image-guided laparoscopic surgery: Comparison with optical tracking and feasibility study of a combined laparoscope and laparoscopic ultrasound system. *Medical physics* 45, 11 (2018), 5094–5104.

[85] Gabriel Zachmann. 1997. Distortion correction of magnetic fields for position tracking. In *Proceedings computer graphics international.* IEEE, 213–220.